SIAM J. APPL. MATH.
Vol. 69, No. 5, pp. 1228–1243

STABILITY OF CURVED INTERFACES IN THE PERTURBED TWO-DIMENSIONAL ALLEN–CAHN SYSTEM*

DAVID IRON†, THEODORE KOLOKOLONIKOV†, JOHN RUMSEY†, AND JUNCHENG WEI‡

Abstract. We consider the singular limit of a perturbed Allen–Cahn model on a bounded two-dimensional domain: $\begin{cases} u_t = \varepsilon^2 \Delta u - 2(u-\varepsilon a)(u^2-1), & x \in \Omega \subset \mathbb{R}^2 \\ \partial_n u = 0, & x \in \partial\Omega \end{cases}$ where ε is a small parameter and a is an $O(1)$ quantity. We study equilibrium solutions that have the form of a curved interface. Using singular perturbation techniques, we fully characterize the stability of such an equilibrium in terms of a certain geometric eigenvalue problem, and give a simple geometric interpretation of our stability results. Full numerical computations of the time-dependent PDE as well as of the associated two-dimensional eigenvalue problem are shown to be in excellent agreement with the analytical predictions.

Key words. Allen–Cahn equation, interface motion, spectral analysis, matched asymptotic expansions

AMS subject classifications. 35B25, 35B32, 35K57

DOI. 10.1137/070706380

1. Introduction.

We consider a perturbed two-dimensional Allen–Cahn equation,

$$\begin{cases} u_t = \varepsilon^2 \Delta u + f(u) + \varepsilon g(u), & x \in \Omega \subset \mathbb{R}^2\,, \\ \partial_n u = 0, & x \in \partial\Omega\,. \end{cases} \tag{1}$$

Here, Ω is a smooth two-dimensional domain and $f(u)$ is a smooth function having the following properties:

1. f has three roots $u_- < u_0 < u_+$ with $f'(u_\pm) < 0$,
2. $\int_{u_-}^{u_+} f(u)\,du = 0$,

and $g(u)$ is any smooth function function with $\int_{u_-}^{u_+} g(u)\,du \neq 0$.

The standard Allen–Cahn equation corresponds to $g = 0$, $f = -2u(u^2-1)$. This model was introduced in [2] as a simple model of evolution of antiphase boundaries and is now well understood. In the limit $\varepsilon \to 0$, the solution forms a sharp interface layer. On one side of the interface, $u \sim u_-$, while on the other, $u \sim u_+$. Once the interface layer is formed, its motion is described by the mean curvature law which minimizes the perimeter of the interface ([5], [9]). The stable stationary solution corresponds to an interface with a minimal perimeter that intersects the boundary orthogonally ([12]). Therefore, any nontrivial stable steady equilibrium of the unperturbed Allen–Cahn equation consists of a straight interface. The stability of such an interface has been analyzed by several authors in variety of settings; see for instance [1], [10], [11], [14], [16], [18]. The main result is that such an interface can be stable provided the domain contains a "neck". More precisely, as shown in [10], [11], in the limit $\varepsilon \to 0$,

*Received by the editors October 25, 2007; accepted for publication (in revised form) September 26, 2008; published electronically February 4, 2009.
http://www.siam.org/journals/siap/69-5/70638.html

†Department of Mathematics and Statistics, Dalhousie University, Halifax, Nova Scotia B3H 4R2, Canada (iron@mathstat.dal.ca, tkolokol@mathstat.dal.ca, John.Rumsey@mathstat.dal.ca).

‡Department of Mathematics, Chinese University of Hong Kong, Shatin, Hong Kong (wei@math.cuhk.edu.hk).

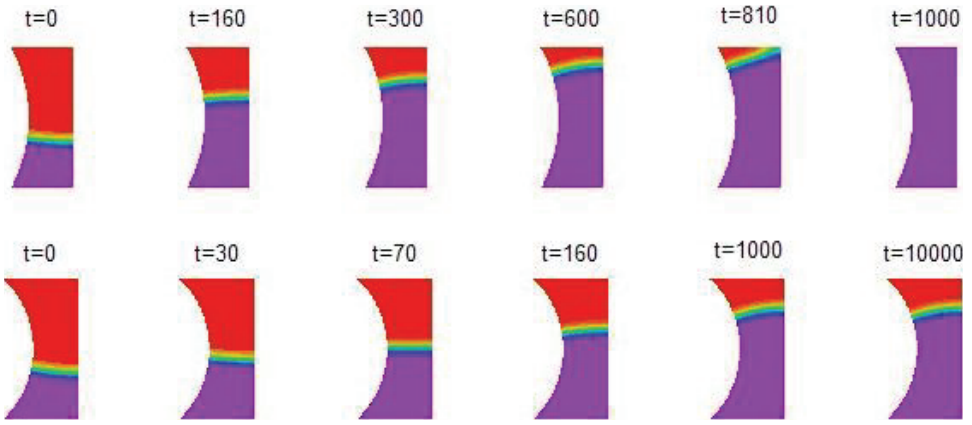

FIG. 1. *Motion of an interface for the perturbed Allen–Cahn model given by* $u_t = \varepsilon^2 \Delta u - 2(u - \varepsilon a)(u^2 - 1)$, *with* $a = 0.3, \varepsilon = 0.07$. *Top row: the interface is unstable and eventually disappears. Bottom row: The interface gets "stuck" in the middle of the domain; a nontrivial equilibrium is reached. The domain height is* 1.5 *and the distance between the side boundaries is* 0.5. *The radius of the left boundary is* 1.5 *for the top row and* 1.0 *for the bottom row.*

the interface stability depends only on the curvatures κ_+, κ_- of the boundary at the two points that intersect the interface, and the interface length ℓ. The interface is stable provided that $\ell + \kappa_+^{-1} + \kappa_-^{-1} < 0$. Geometrically, the threshold case corresponds to the two boundaries that are locally concentric.

More generally, the perturbed Allen–Cahn equation (1) is used as a prototype model of wave propagation in various contexts. In two or higher dimensions, a small perturbation leads to *weakly curved fronts*. For an overview, see [15], Chapter 2.2. In the absence of boundaries, the front becomes a closed curve which lies on a perimeter of some circle. Moreover, such a front is unstable, and either shrinks to a point or else expands indefinitely, depending on the initial conditions [15]. A typical nonlinearity is $f + \varepsilon g = -2(u - A)(u^2 - 1)$ where A is close to 0. This system (but without the assumption that A is small) was used as a simple model of spreading depressions in the human brain that are associated with cerebral strokes [4]. (When A is replaced by an inhomogeneous term $a(x)$, it is called the Fife–Greenlee problem [8], [6].) For convex domains, it is known ([3] [13]) that the only stable solution is a trivial equilibrium. Indeed any interface propagates until it merges with the boundary and disappears.

However, when the domain consists of two boxes of different heights, it was shown in [4] that the interface can get "stuck" at the juncture between the two boxes, provided their dimensions are sufficiently different. A similar phenomenon was reported in [17], where the propagation of chemical pulses in complex geometries with corners and junctures was studied numerically and experimentally.

The perturbation by a small term $\varepsilon g(u)$ has a large effect on the shape and stability of the interface. In particular, the equilibrium solution now consists of a *curved* interface. In the limit $\varepsilon \to 0$, this curve is part of a circular arc whose radius $\hat{R}$, given by (2) below and is independent of the domain shape. For non-convex domains, it is possible to get a stable interface. One such domain is illustrated in Figure 1. It consists of a rectangle with a circular cutout. In the first simulation (top row), the interface propagates through the domain without reaching any equilibrium, whereas in the second simulation (second row) the interface settles to a steady state somewhere in the middle of the domain. The only difference between the two simulations is the

curvature of the left boundary of the domain, which has been increased in the second simulation.

In this paper, we fully characterize the stability of curved interfaces. First, we provide the necessary and sufficient conditions that describe the stability of an interface. Second, we give a simple geometric interpretation of our stability results.

Before stating our stability result, we characterize the radius of the steady state. This simple result was already given in [16], Appendix A. We summarize it here as following.

PROPOSITION 1. *Let U be a solution to*

$$U''(y) + f(U) = 0, \qquad U \to u_\pm \quad \text{as } y \to \pm\infty$$

and define

$$\hat{R} = -\frac{\int_{-\infty}^{\infty} U'^2(y)dy}{\int_{u_-}^{u_+} g(u)du}. \tag{2}$$

Suppose that there exists a circle of radius $\hat{R}$ which intersects $\partial\Omega$ orthogonally, and let p be its center. Then in the limit $\varepsilon \to 0$ we have

$$u(x) \sim U\left(\frac{\hat{R} - |p - x|}{\varepsilon}\right), \quad \varepsilon \to 0. \tag{3}$$

Moreover, any solution to (1) *of the form* (3) *must satisfy* (2).

We are now ready to state our main result.

THEOREM 2. *Let $u(x)$ be the steady-state solution as given in Proposition* 1 *and $\hat{R}$ its radius as defined in* (2). *Let ℓ be the length of the interface and let κ_+, κ_- be the curvatures of the boundary at the points which intersect the interface. Consider the stability problem associated with* (1),

$$\begin{cases} \lambda\phi = \varepsilon^2\Delta\phi + f'(u)\phi + \varepsilon g'(u)\phi, & x \in \Omega \\ \partial_n\phi = 0, & x \in \partial\Omega. \end{cases} \tag{4}$$

In the limit $\varepsilon \to 0$, the eigenvalues λ are of $O(\varepsilon^2)$ given by

$$\lambda = \varepsilon^2\lambda_0, \tag{5a}$$

where λ_0 solves the following geometric eigenvalue problem*:*

$$\begin{cases} T'' + \left(\hat{R}^{-2} - \lambda_0\right)T = 0 \\ T'(-\ell/2) + \kappa_- T(-\ell/2) = 0 \\ T'(\ell/2) - \kappa_+ T(\ell/2) = 0. \end{cases} \tag{5b}$$

Thus, the interface is stable if all solutions λ_0 of (5b) *are negative, and unstable if at least one solution is positive. Equivalently, λ_0 solves*

$$\lambda_0 = \frac{1}{\hat{R}^2} - \mu^2 \quad \text{where} \quad \tan(\mu\ell) = -\frac{\mu(\kappa_+ + \kappa_-)}{\mu^2 - \kappa_+\kappa_-} \tag{6}$$

or

$$\arctan\left(\frac{-\kappa_+}{\mu}\right) + \arctan\left(\frac{-\kappa_-}{\mu}\right) = \mu\ell \tag{7}$$

for some branch of arctan.

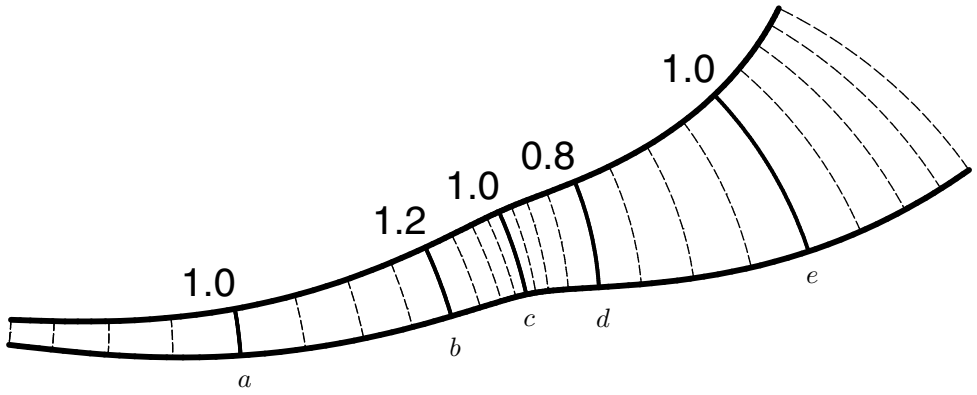

FIG. 2. *Geometric interpretation of stability criterion (see Theorem 3). The numbers indicate the radius of the corresponding interface below that number. The maximum and minimum radius is* 1.2 *and* 0.8*, respectively. If* $\hat{R} = 1$*, then curve c represents the location of a stable interface, whereas curves a and e correspond to unstable interfaces.*

Remark. Suppose that $\lambda_0 \neq 0$, i.e., the geometric eigenvalue problem (5b) has no zero eigenvalue. Then the existence of such steady state can be rigorously proved, following the lines of [11]. We omit the details.

In the case of the unperturbed Allen–Cahn equation ($g = 0, \quad \hat{R} = \infty$), the geometric eigenvalue problem (5b) is identical to (1.5) obtained by Kowalczyk in [10], [11]. However, here we use a somewhat different method using solvability condition and test functions.

The stability criterion (5b) has a natural geometric interpretation which we now discuss. Consider a domain such as shown in Figure 2. Parameterize the top boundary in terms of arclength s, from left to right, and let $q(s)$ be the corresponding point on the top boundary. We suppose that there is a unique circle that goes through $q(s)$ and that intersects both top and bottom boundaries orthogonally. Let $R(s)$ denote the radius of such a circle. Then we have the following.

THEOREM 3. *Let* $\hat{R}$ *be the radius of a steady interface as defined in Proposition* 1*, let* $R(s)$ *be as defined above, and suppose that* $R(s) = \hat{R}$ *for some* s*. Then the interface is stable if* $R'(s) < 0$ *and it is unstable if* $R'(s) > 0$*.*

For example, for the domain as shown in Figure 2, if $\hat{R} \in (0.8, 1.2)$, then there exists a stable steady interface between curves b and d. On the other hand, any interface to the left of b or to the right of d is unstable. To our knowledge, this is the first result that combines both the effects of perturbation and the effects of the boundary.

The rest of the paper is outlined as follows. Proposition 1 is derived in section 2. The main result, Theorem 2, is then derived in section 3. Finally we prove Theorem 3 in section 4. We conclude with numerical calculations in section 5 and some discussions and open problems in section 6.

2. Equilibrium front solution. In this section we construct the steady state consisting of a single interface. The main goal is to derive (2) of Proposition 1.

We seek a solution which divides the domain into two regions. In one of the regions $u \sim u_+$ and in the other $u \sim u_-$. The two regions are separated by an interface, or front, of thickness $O(\varepsilon)$. We expect the interface to be localized about a circle segment which intersects the boundary of Ω orthogonally. Let $\hat{R}$ be the radius

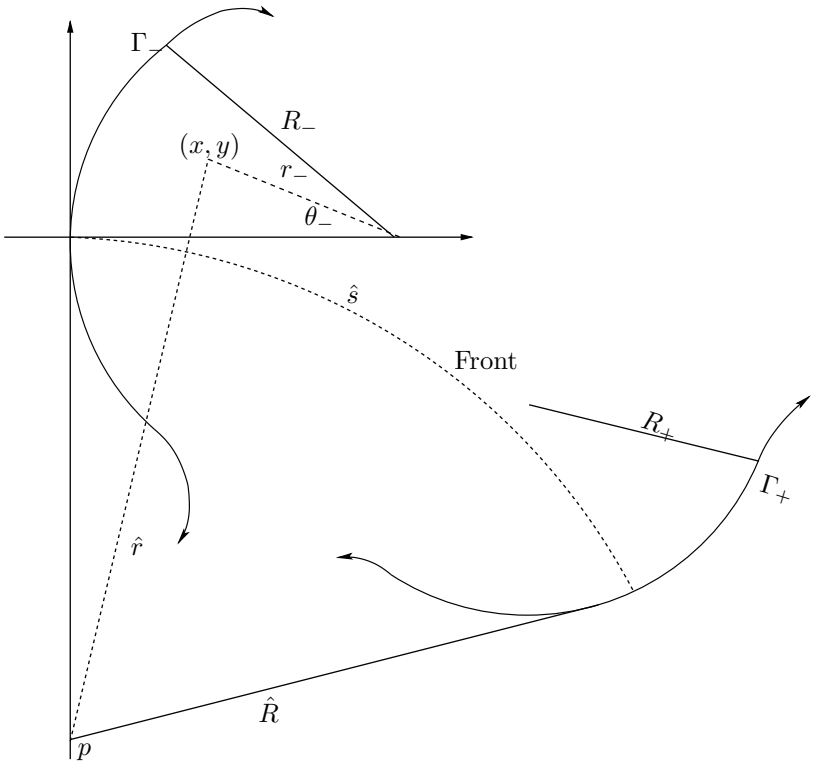

FIG. 3. *Schematic used for the derivation of coordinate systems in the interior of the domain and localized near the boundaries.*

of the interface and define the following coordinate system as illustrated in Figure 3:

$$x = R_- - r_- \cos(\theta_-) = \hat{r}\sin(\hat{s}/\hat{R})\,, \tag{8}$$

$$y = r_- \sin(\theta_-) = \hat{r}\cos(\hat{s}/\hat{R}) - \hat{R}\,. \tag{9}$$

Near the boundaries, we define localized coordinates $\rho_\pm$ and $t_\pm$ as follows:

$$\rho_\pm \equiv \frac{r_\pm - R_\pm}{\varepsilon}\,, \qquad t_\pm \equiv \frac{R_\pm \theta_\pm}{\varepsilon}\,. \tag{10}$$

Here, $+$ and $-$ are used to denote the right and left curved boundaries, respectively. The $\pm$ will be dropped whenever the meaning is clear. We also define coordinates localized near the front by

$$\hat{\rho} \equiv \frac{\hat{r} - \hat{R}}{\varepsilon}\,. \tag{11}$$

We can then write $\hat{\rho}$ as a function of t and ρ:

$$\hat{\rho} = t - \varepsilon\left(\frac{\rho t}{R} - \frac{\rho^2}{2\hat{R}}\right) + \cdots\,. \tag{12}$$

In the interior of the domain, we expect the front to be radially symmetric. Thus, in the new coordinate system, the equilibrium front will satisfy

$$u_{\hat{\rho}\hat{\rho}} + \frac{\varepsilon}{\hat{R} + \varepsilon\hat{\rho}} u_{\hat{\rho}} + f(u) + \varepsilon g(u) = 0\,, \tag{13}$$

in the interior of the domain. We expand

$$u = u_0 + \varepsilon u_1 + \varepsilon^2 u_2 + \cdots , \tag{14}$$

substitute into (13), and collect powers of ε to obtain,

$$u_0'' + f(u_0) = 0 , \tag{15}$$

$$u_1'' + f'(u_0)u_1 = -\frac{1}{\hat{R}}u_0' - g(u_0) , \tag{16}$$

$$u_2'' + f'(u_0)u_2 = \frac{1}{\hat{R}^2}\hat{\rho}u_0' - \frac{1}{\hat{R}}u_1' - \frac{f''(u_0)u_1^2}{2} - g'(u_0)u_1 . \tag{17}$$

From here on $'$ denotes differentiation with respect to $\hat{\rho}$ when associated with u_i. In all other cases $'$ will represent differentiation with respect to the appropriate argument. At this point it is convenient to define the operator $L\psi \equiv \psi'' + f'(u_0)\psi$.

From conditions 1 and 2 following (1), u_0 will be given by the unique heteroclinic orbit connecting u_+ to u_-. For the case $f(u) = 2u(1-u^2)$, we have the exact solution $u_0 = \tanh(\hat{\rho})$. We note that by differentiating (15) with respect to $\hat{\rho}$, $Lu_0' = 0$.

To determine $\hat{R}$, we consider the steady-state system,

$$\varepsilon^2 \Delta u + f(u) + \varepsilon g(u) = 0 . \tag{18}$$

We multiply (18) by u_0' and integrate over the domain,

$$\int_\Omega u_0'(\varepsilon^2 \Delta u + f(u) + \varepsilon g(u))\, dA = 0 . \tag{19}$$

Applying Green's identity to (19) we obtain

$$-\varepsilon^2 \int_{\partial\Omega} u\, \partial_n u_0'\, ds + \int_\Omega \varepsilon^2 u\, \Delta(u_0') + u_0'(f(u) + \varepsilon g(u))\, dA = 0 . \tag{20}$$

We now use (14) and (11) in (20) and collect powers of ε to obtain

$$\begin{aligned} -\varepsilon^2 \int_{\partial\Omega} u_0 \partial_n u_0'\, ds + \int_\Omega \Big(& (u_0(u_0')'' + f(u_0)u_0') + \varepsilon \\ & \left((u_0')'' u_1 + \frac{1}{\hat{R}}(u_0')' u_0 + f'(u_0)u_1 u_0' + g(u_0)u_0' \right) \Big)\, dA = 0 . \end{aligned} \tag{21}$$

Integrating over $\hat{\rho}$ by parts and using $\lim_{\hat{\rho}\to\pm\infty} u_0' = 0$ yields

$$\int_\Omega (u_0')'' u_0\, dA = \int_\Omega u_0'' u_0'\, dA , \tag{22}$$

$$\int_\Omega (u_0')' u_0\, dA = \int_\Omega (u_0')^2\, dA . \tag{23}$$

Using (15) and $Lu_0 = 0$, (21) may be written as

$$-\varepsilon \int_{\partial\Omega} \partial_n u_0' u_0\, ds = -\int_\Omega \left(\frac{u_0'}{\hat{R}} + g(u_0) \right) u_0'\, dA . \tag{24}$$

Using (12) we find the leading order behavior of $\partial_n u_0'|_{\partial\Omega}$:

$$\partial_n u_0'|_{\partial\Omega} \sim \frac{\partial}{\partial\rho} u_0' \left(t - \varepsilon \left(\frac{\rho t}{R} - \frac{\rho^2}{2\hat{R}} \right) \right) \Big|_{\rho=0}, \tag{25}$$

$$= -\varepsilon u_0'' \frac{t}{R}. \tag{26}$$

Thus, the boundary term in (24) is of a much lower order, and the equilibrium radius of the front is given by

$$\hat{R} \sim -\frac{\int_{-\infty}^{\infty} (u_0')^2 \, dt}{\int_{u_-}^{u_+} g(y) \, dy}. \tag{27}$$

This shows, that to leading order, $\hat{R}$ is independent of the domain shape and completes the derivation of Proposition 1.

3. Proof of Theorem 2. We now construct a solvability condition to determine the principal eigenvalues of (4). Since u_0' is of one sign and $Lu_0' = 0$, we expect that the principal eigenvalue is small and to leading order the principal eigenfunction will behave like u_0' in the interior of the domain. Such an eigenfunction is often referred to as a translation eigenfunction as it is associated with the near translation invariance of the front in the interior of the domain with respect to the radial co-ordinate. In this case, $\hat{s}u_0'$ also satisfies (4) to leading order and as a result, we will need two solvability conditions to determine the principal eigenvalue.

We construct our solvability conditions by multiplying (4) by test function v and integrating over the domain we obtain

$$\int_\Omega v \left(\varepsilon^2 \Delta\phi + f'(u)\,\phi \right) dA + \varepsilon \int g'(u)\,\phi\, v \, dA = \lambda \int_\Omega \phi\, v \, dA, \tag{28}$$

where v is of the form

$$v(\hat{s}, \hat{\rho}) = w(\hat{s})\, u_0'(\hat{\rho}) \tag{29}$$

and $w(\hat{s})$ is an arbitrary test function.

Using Green's identity and applying the boundary conditions in (4) results in

$$-\varepsilon^2 \int_{\partial\Omega} \phi\, \partial_n v \, ds + \int_\Omega \Big(\varepsilon^2 \Delta v + f'(u)\, v + \varepsilon\, g'(u)\, v \Big) \phi \, dA = \lambda \int_\Omega \phi\, v \, dA. \tag{30}$$

Here, s is arc length along the boundary and dA is an element of area in the interior. From (10) and (11),

$$ds = R\, d\theta = \varepsilon\, dt, \tag{31}$$

$$dA = \frac{\hat{r}}{\hat{R}}\, d\hat{r}\, d\hat{s} = \varepsilon \left(1 + \varepsilon \frac{\hat{\rho}}{\hat{R}} \right) d\hat{\rho}\, d\hat{s}. \tag{32}$$

Consider the $\int_\Omega \Big(\varepsilon^2 \Delta v + f'(u)\, v + \varepsilon\, g'(u)\, v \Big) \phi \, dA$ term in (30), in which v, u, ϕ are written in the interior coordinates $\hat{r}$ and $\hat{s}$. Expand ϕ:

$$\phi = \phi_0 + \varepsilon \phi_1 + \varepsilon^2 \phi_2 + \cdots. \tag{33}$$

Use (11), (32), (33), and (14) to write $\int_\Omega \Big(\varepsilon^2\Delta v + f'(u)\,v + \varepsilon\, g'(u)\,v\Big)\phi\, dA$ in terms of the coordinates, $\hat\rho$ and $\hat s$:

$$
\begin{aligned}
&\Big(\varepsilon^2\Delta v(\hat r) + f'(u)\,v(\hat r) + \varepsilon\, g'(u)\,v(\hat r)\Big)\phi\, dA\\
&\quad\sim \left[\varepsilon^2\left(\frac{1}{\varepsilon^2}\,v_{\hat\rho\hat\rho} + \frac{1}{\hat R+\varepsilon\hat\rho}\,\frac{1}{\varepsilon}v_{\hat\rho} + v_{\hat s\hat s}\right) + f'\left(u_0+\varepsilon\,u_1+\varepsilon^2\,u_2\right)\,v\right.\\
&\qquad\left. +\ \varepsilon\, g'\left(u_0+\varepsilon\,u_1+\varepsilon^2\,u_2\right)\,v\right]\left[\phi_0+\varepsilon\phi_1+\varepsilon^2\phi_2\right]\left[\varepsilon\left(1+\varepsilon\,\frac{\hat\rho}{\hat R}\right)d\hat\rho\, d\hat s\right]\\
&\quad\sim \left\{\varepsilon^2\left[\frac{1}{\hat R}\,v_{\hat\rho}\,\phi_0 + u_1\,f''(u_0)\,v\,\phi_0 + g'(u_0)\,v\,\phi_0\right]\right.\\
&\qquad +\varepsilon^3\left[v_{\hat s\hat s}\phi_0 + u_2\,f''(u_0)\,v\,\phi_0 + \frac{1}{2}\,u_1^2\,f'''(u_0)\,v\,\phi_0 + u_1\,g''(u_0)\,v\,\phi_0\right.\\
&\qquad\quad + \frac{1}{\hat R}\,v_{\hat\rho}\,\phi_1 + u_1\,f''(u_0)\,v\,\phi_1 + g'(u_0)\,v\,\phi_1\\
&\qquad\quad \left.\left. + \frac{\hat\rho}{\hat R}\,u_1\,f''(u_0)\,v\,\phi_0 + \frac{\hat\rho}{\hat R}\,g'(u_0)\,v\,\phi_0\right]\right\} d\hat\rho\, d\hat s
\end{aligned}
\tag{34}
$$

since $v = w(\hat s)u_0'(\hat\rho)$ is in the kernel of L.

Equation (34) has terms involving u_1 and u_2, so we must examine (16) and (17) for these terms. We take the derivative of (16) with respect to $\hat\rho$ and multiply by $w\phi_0$, integrate, and use Green's identity to obtain

$$
\int_{\partial\Omega}\partial_n u_1' w\phi_0\, ds = \int_\Omega\left(-\frac{1}{\hat R}u_0'' - f''(u_0)u_0'u_1 - g'(u_0)u_0'\right)w\phi_0\, dA\,. \tag{35}
$$

It will become evident that $\lambda = O(\varepsilon^2)$. To avoid tedious calculations, we will write $\lambda = \varepsilon^2\lambda_0 + \cdots$. In this way, λ_0 terms will enter at the correct order. We substitute (31) and (32) into (35), multiply by ε, and arrange the terms to match the u_1 term in (34):

$$
\begin{aligned}
&\varepsilon^2\int_\Omega f''(u_0)u_0'u_1 w\phi_0\, d\hat\rho\, d\hat s\\
&\qquad = -\,\varepsilon^2\left(\int_\Omega\left(\frac{1}{\hat R}u_0'' + g'(u_0)\,u_0'\right)w\phi_0\, d\hat\rho\, d\hat s + \int_{\partial\Omega}\partial_n u_1' w\phi_0\, dt\right)\\
&\qquad\quad +\varepsilon^3\int_\Omega\left(-\frac{1}{\hat R}u_0'' - f''(u_0)u_0'u_1 - g'(u_0)\,u_0'\right)\frac{\hat\rho}{\hat R}w\phi_0\, d\hat\rho\, d\hat s + \cdots\,.
\end{aligned}
\tag{36}
$$

We repeat the above procedure to handle the u_2 term in (34). First we differentiate (17) with respect to $\hat\rho$,

$$
\begin{aligned}
\Delta(u_2') + f'(u_0)u_2' = &-\frac{1}{\hat R}u_1'' + \frac{1}{\hat R^2}\hat\rho u_0'' + \frac{1}{\hat R^2}u_0' - f''(u_0)u_0'u_2\\
&-\frac{f'''(u_0)u_0'u_1^2}{2} - f''(u_0)u_1u_1' - g''(u_0)u_0'u_1 - g'(u_0)u_1'\,.
\end{aligned}
\tag{37}
$$

We multiply the above expression by ϕ_0, integrate over the domain, apply Green's identity to the right-hand side, and multiply by ε^3 to match the u_2 term in (34) which

results in the following:

$$\varepsilon^3\int_\Omega f''(u_0)u_0'u_2w\phi_0\,d\hat\rho\,d\hat s = \varepsilon^3\int_\Omega\left(-\frac{1}{\hat R}u_1'' + \frac{1}{\hat R^2}\hat\rho u_0'' + \frac{1}{\hat R^2}u_0' - \frac{f'''(u_0)u_0'u_1^2}{2}\right.$$
$$\left. - f''(u_0)u_1u_1' - g''(u_0)u_0'u_1 - g'(u_0)u_1'\right)w\phi_0\,d\hat\rho\,d\hat s$$
$$+\varepsilon^3\int_{\partial\Omega}\partial_n u_2'w\phi_0\,dt + \cdots\,. \tag{38}$$

Since ϕ is a translation eigenfunction, in the interior we may write

$$\phi_i = T(\hat s)u_i'(\hat\rho). \tag{39}$$

We also note that

$$\int_\Omega \frac{1}{\hat R}u_1''w\phi_0\,d\hat\rho\,d\hat s = -\int_\Omega\frac{1}{\hat R}w\phi_0'u_1'\,d\hat\rho\,d\hat s\,. \tag{40}$$

Using (40), (39), (38), (36), and (34) we can write (28) as

$$\varepsilon^2\lambda_0\int_\Omega v\phi_0\,d\hat\rho\,d\hat s$$
$$= \varepsilon^2\int_\Omega\left(v_{\hat s\hat s}\phi_0 + \frac{2}{\hat R}\phi_1v_{\hat\rho} + \frac{1}{\hat R^2}w\phi_0\right)d\hat\rho\,d\hat s - \varepsilon^2\int_{\partial\Omega}(\phi_0\partial_n v + w\phi_0\partial_n u_1')\,dt + \cdots\,, \tag{41}$$

where, from (38), the boundary integral involving $\partial_n u_2'$ is of higher order. The eigenfunction $\phi_0 = T(\hat s)u_0'$ is the derivative of a monotonic front and is, thus, of one sign and hence is the principal eigenfunction. The principal eigenfunction of L must be even in the radial direction and the function v' will be odd in the radial direction. Thus, the term $\int_\Omega \frac{2}{\hat R}\phi_1v'\,d\hat\rho\,d\hat s$ will be zero to leading order.

For the boundary integral involving $\partial_n v$, we need to find $\partial_n v$ on $\partial\Omega$. Away from the points where the front and boundary intersect, $\partial_n v$ will be exponentially small, so we will only consider the two components of the boundary $\Gamma_\pm$. Since the front meets $\Gamma_\pm$ orthogonally,

$$\partial_n v|_{\Gamma_\pm} = \left.\frac{\partial v}{\partial r}\right|_{\Gamma_\pm}. \tag{42}$$

We note from (8), (9), (10), and (11),

$$\left.\frac{\partial\hat s}{\partial r}\right|_{\Gamma_\pm} \sim \pm 1 \quad\text{and}\quad \left.\frac{\partial\hat\rho}{\partial r}\right|_{\Gamma_\pm} \sim \left.\frac{t}{R}\right|_{\Gamma_\pm}. \tag{43}$$

Thus,

$$\partial_n v\big|_{\Gamma_\pm} \sim \left.\left(\pm w'(\hat s)u_0'(t) + w(\hat s)u_0''(t)\frac{t}{R}\right)\right|_{\Gamma_\pm}. \tag{44}$$

We let ℓ be the length of the interface and place $\hat s = 0$ such that $\hat s = \pm\ell/2$ on $\Gamma_\pm$. Then, using (39), (29), $\hat\rho\sim t$ on $\Gamma_\pm$ and $\int tu_0''u_0 = -\frac{1}{2}\int {u_0'}^2$ with (44) results in

$$-\int_{\partial\Omega}\partial_n v\phi_0\,dt \sim w'(-\ell/2)T(-\ell/2)\int_{-\infty}^{\infty}(u_0'(t))^2\,dt + \frac{w(-\ell/2)T(-\ell/2)}{2R_-}\int_{-\infty}^{\infty}(u_0'(t))^2\,dt$$
$$- w'(\ell/2)T(\ell/2)\int_{-\infty}^{\infty}(u_0'(t))^2\,dt + \frac{w(\ell/2)T(\ell/2)}{2R_+}\int_{-\infty}^{\infty}(u_0'(t))^2\,dt\,. \tag{45}$$

For the boundary integral involving $\partial_n u_1'$, we have that, near $\partial\Omega$,

$$u \sim u_0(\hat{\rho}) + \varepsilon\, u_1 = u_0(t) + \varepsilon \left(\frac{\rho\, t}{R} + \frac{\rho^2}{2\hat{R}} \right) u_0'(t) + \varepsilon\, u_1 + \cdots . \tag{46}$$

Also, on $\partial\Omega$, we have $\partial_n u = 0$, so that, on $\partial\Omega$

$$\partial_n u_1 \sim - \frac{\partial}{\partial \rho} \left[\frac{1}{\varepsilon}\, u_0(t) + \left(\frac{\rho\, t}{R} + \frac{\rho^2}{2\hat{R}} \right) u_0'(t) \right] \Big|_{\rho=0} = - \frac{t}{R}\, u_0'(t) \Big|_{\Gamma_\pm} . \tag{47}$$

Then

$$\partial_n u_1' \sim - \frac{1}{R}\, u_0'(t) - \frac{t}{R}\, u_0''(t) \tag{48}$$

and

$$\begin{aligned} - \int_{\partial\Omega} \partial_n u_1' w \phi_0 \, dt \sim & \int_{\Gamma_-} w(-\ell/2) T(-\ell/2) \left(u_0''(t) u'(t) \frac{t}{R} + u_0'(t)^2 \frac{1}{R} \right) dt \\ & + \int_{\Gamma_+} w(\ell/2) T(\ell/2) \left(u_0''(t) u'(t) \frac{t}{R} + u_0'(t)^2 \frac{1}{R} \right) dt \,, \\ = & \left(\frac{w(\ell/2) T(\ell/2)}{2R_+} + \frac{w(-\ell/2) T(-\ell/2)}{2R_-} \right) \int_{-\infty}^{\infty} (u_0'(t))^2 \, dt \,. \end{aligned} \tag{49}$$

Substitute (44) and (49) into (41) to obtain

$$\begin{aligned} \left(\lambda_0 - \frac{1}{\hat{R}^2} \right) \int_\Omega v \phi_0 \, d\hat{\rho}\, d\hat{s} \sim & \int_\Omega v_{\hat{s}\hat{s}} \phi_0 \, d\hat{\rho}\, d\hat{s} + \left(w'(-\ell/2) T(-\ell/2) + \frac{w(-\ell/2) T(-\ell/2)}{2R_-} \right. \\ & \left. - w'(\ell/2) T(\ell/2) + \frac{w(\ell/2) T(\ell/2)}{2R_+} \right) \int_{-\infty}^{\infty} (u_0'(t))^2 \, dt \,. \end{aligned} \tag{50}$$

The eigenfunctions will depend on both $\hat{s}$ and $\hat{\rho}$. We thus substitute the ansatz $\phi = T(\hat{s})\Phi(\hat{\rho})$ into the eigenvalue problem (4),

$$\left(\Phi'' + \frac{\varepsilon}{\hat{R}} \Phi' - \varepsilon^2 \frac{\hat{\rho}}{\hat{R}^2} \Phi' + f'(u)\Phi + \varepsilon g'(u)\Phi \right) T + \varepsilon^2 T'' \Phi = \varepsilon^2 \lambda_0 T \Phi \,. \tag{51}$$

We divide both sides by $T\Phi$,

$$\left(\frac{\Phi'' + \frac{\varepsilon}{\hat{R}} \Phi' - \varepsilon^2 \frac{\hat{\rho}}{\hat{R}^2} \Phi' + f'(u)\Phi + \varepsilon g'(u)\Phi}{\Phi} \right) + \varepsilon^2 \frac{T''}{T} = \varepsilon^2 \lambda_0 \,. \tag{52}$$

Since T is independent of $\hat{\rho}$, the term in the brackets must be independent of $\hat{\rho}$ or equal to a constant α:

$$\Phi'' + \frac{\varepsilon}{\hat{R}} \Phi' - \varepsilon^2 \frac{\hat{\rho}}{\hat{R}^2} \Phi' + f'(u)\Phi + \varepsilon g'(u)\Phi = \alpha \Phi \,. \tag{53}$$

We expand $\Phi = \Phi_0 + \varepsilon\Phi_1 + \varepsilon^2\Phi_2 + \cdots$ and $\alpha = \alpha_0 + \varepsilon\alpha_1 + \varepsilon\alpha_2 + \cdots$. The lowest order terms satisfy

$$\Phi_0'' + f'(u_0)\Phi_0 = \alpha_0 \Phi_0 \,. \tag{54}$$

Thus, $\Phi_0 = u_0'(\hat{\rho})$ and $\alpha_0 = 0$. The $O(\varepsilon)$ terms satisfy

$$\Phi_1'' + f'(u_0)\Phi_1 = \alpha_1\Phi_0 - \frac{1}{\hat{R}}\Phi_0' - f''(u_0)u_1\Phi_0 - g'(u_0)\Phi_0\,. \tag{55}$$

Differentiating (16) results in the following solvability condition,

$$\int_{-\infty}^{\infty} f''(u_0)u_1(u_0')^2\,d\hat{\rho} = -\int_{-\infty}^{\infty} g'(u_0)(u_0')^2\,d\hat{\rho}\,. \tag{56}$$

Applying (56) to the solvability condition for (55) yields $\alpha_1 = 0$. The $O(\varepsilon^2)$ terms satisfy

$$\begin{aligned}\Phi_2'' + f'(u_0)\Phi_2 = \alpha_2\Phi_0 - \Phi_1'\frac{1}{\hat{R}} + \frac{1}{\hat{R}^2}\hat{\rho}\Phi_0' \\ - f''(u_0)u_1\Phi_1 - f''(u_0)u_2\Phi_0 - \frac{1}{2}f'''(u_0)u_1^2\Phi_0 - g''(u_0)u_1\Phi_0 - g'(u_0)\Phi_1\,.\end{aligned} \tag{57}$$

We have the following solvability condition:

$$\begin{aligned}\alpha_2\int_{-\infty}^{\infty}\Phi_0^2\,d\hat{\rho} =& \frac{1}{2}\int_{-\infty}^{\infty} f'''(u_0)u_1^2\Phi_0^2\,d\hat{\rho} + \int_{-\infty}^{\infty} g''(u_0)u_1\Phi_0^2\,d\hat{\rho} + \int_{-\infty}^{\infty} g'(u_0)\Phi_1\Phi_0\,d\hat{\rho} \\ &+ \int_{-\infty}^{\infty} f''(u_0)u_2\Phi_0^2\,d\hat{\rho} + \int_{-\infty}^{\infty} f''(u_0)u_1\Phi_1\Phi_0\,d\hat{\rho} - \int_{-\infty}^{\infty}\frac{1}{\hat{R}^2}\hat{\rho}\Phi_0'\Phi_0\,d\hat{\rho} \\ &+ \int_{-\infty}^{\infty}\frac{1}{\hat{R}}\Phi_1'\Phi_0\,d\hat{\rho}\,.\end{aligned} \tag{58}$$

Differentiating (17) results in the solvability condition,

$$\begin{aligned}&-\int_{-\infty}^{\infty} f''(u_0)u_2(u_0')^2\,d\hat{\rho} - \int_{-\infty}^{\infty}\frac{1}{\hat{R}}u_1''u_0'\,d\hat{\rho} + \frac{1}{\hat{R}^2}\int_{-\infty}^{\infty}\hat{\rho}u_0''u_0'\,d\hat{\rho} + \frac{1}{\hat{R}^2}\int_{-\infty}^{\infty}(u_0')^2\,d\hat{\rho} \\ &-\int_{-\infty}^{\infty} f''(u_0)u_1u_1'u_0'\,d\hat{\rho} - \frac{1}{2}\int_{-\infty}^{\infty} f'''(u_0)u_1^2(u_0')^2\,d\hat{\rho} - \int_{-\infty}^{\infty} g''(u_0)u_1(u_0')^2\,d\hat{\rho} \\ &- \int_{-\infty}^{\infty} g'(u_0)u_1'u_0'\,d\hat{\rho} = 0\,.\end{aligned} \tag{59}$$

Now we use $\int_{-\infty}^{\infty}\hat{\rho}u_0''u_0'\,d\hat{\rho} = -\frac{1}{2}\int_{-\infty}^{\infty}(u')^2\,d\hat{\rho}$ and (58) in (57) to yield

$$\alpha_2 = \frac{1}{\hat{R}^2}\,. \tag{60}$$

Now we can substitute (53) into (52) using $\alpha = \frac{\varepsilon^2}{\hat{R}^2} + \cdots$ to get

$$T'' = \left(\lambda_0 - \frac{1}{\hat{R}^2}\right)T\,. \tag{61}$$

Note that

$$\left(\lambda_0 - \frac{1}{\hat{R}^2}\right)\int_\Omega v\phi_0\, d\hat{\rho}\, d\hat{s} \sim \left(\lambda_0 - \frac{1}{\hat{R}^2}\right)\int_{-\ell/2}^{\ell/2} wT d\hat{s} \int_{-\infty}^{\infty} (u_0'(t))^2\, dt \tag{62}$$

$$\int_\Omega v_{\hat{s}\hat{s}}\phi_0 \sim \int_{-\ell/2}^{\ell/2} w^{''} T d\hat{s} \int_{-\infty}^{\infty} (u_0'(t))^2\, dt\,. \tag{63}$$

Substituting (61), (62), and (63) into (50), integrating by parts, we obtain

$$w(-\ell/2)\left[T^{'}(-\ell/2) + \frac{1}{R_-}T(-\ell/2)\right] + w(\ell/2)\left[-T^{'}(\ell/2) + \frac{1}{R_+}T(\ell/2)\right] = 0.$$

Since w is an arbitrary test function, we see that T satisfies the following boundary conditions:

$$T^{'}(-\ell/2) + \frac{1}{R_-}T(-\ell/2) = 0,\ -T^{'}(\ell/2) + \frac{1}{R_+}T(\ell/2) = 0. \tag{64}$$

Equations (61) and (64) prove that T satisfies the geometric eigenvalue problem (5b). Hence, $\lambda_0 = \frac{1}{\hat{R}^2} - \alpha$ where α satisfies

$$\begin{cases} T'' + \alpha T = 0, \\ T'(-\ell/2) + \kappa_- T(-\ell/2) = 0, \\ T'(\ell/2) - \kappa_+ T(\ell/2) = 0, \end{cases} \tag{65}$$

where $\kappa_\pm \equiv \frac{1}{R_\pm}$ and $\kappa_\pm > 0$ corresponds to a convex domain as in Figure 3.

If $\alpha \le 0$, then $\lambda_0 \ge \frac{1}{\hat{R}^2}$. If $\alpha = \mu^2 > 0$, (where $\mu > 0$), then it is easy to see that μ must satisfy the following transcendental relation:

$$\tan(\mu\ell) = \frac{\mu(\kappa_+ + \kappa_-)}{\kappa_+\kappa_- - \mu^2}\,, \tag{66}$$

and the eigenvalues of (4) are given by

$$\varepsilon^2\lambda = \frac{1}{\hat{R}} - \mu^2\,, \tag{67}$$

which is precisely (6). Formula (7) is seen to be identical to (6) by applying the identity

$$\tan(x+y) = \frac{\tan x + \tan y}{1 - \tan x \tan y}. \tag{68}$$

This completes the proof of Theorem 2. □

4. Proof of Theorem 3. In this section we show that the geometric condition of Theorem 3 is a direct consequence of Theorem 2.

Fix a point q_+ on the top boundary and consider a circular arc going through q_+ and intersecting both top and bottom boundaries orthogonally (refer to Figure 4). Let p be the center of this arc and let R denote its radius. First, we shall show that $\frac{dR}{dq_+} = 0$ if and only if the formula (5) holds with $\lambda_0 = 0$. By zooming into the point where $\frac{dR}{dq_+} = 0$, we can assume that locally, p moves along a straight line as q_+ moves along the boundary, and that the boundaries are segments of circles of radii $\mathcal{R}_\pm$, as

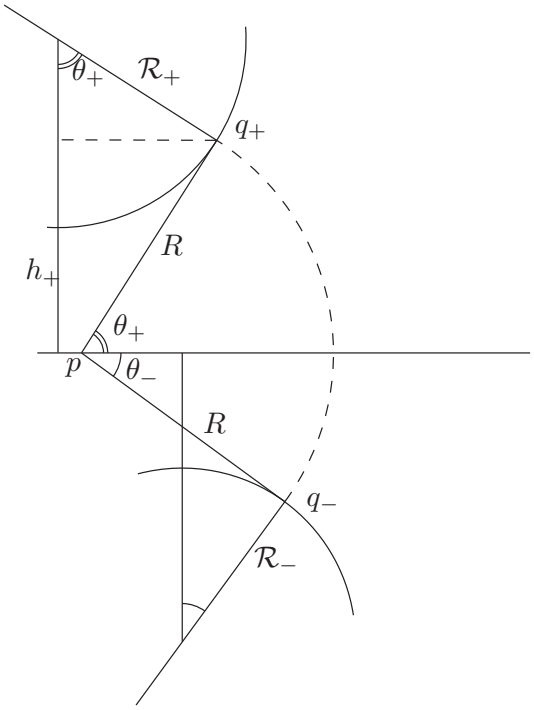

FIG. 4. *Setup for proof of Theorem* 3.

shown in Figure 4. In general, $\mathcal{R}_\pm$ may be positive or negative; for convenience, as shown in the figure, we chose $\mathcal{R}_\pm = -\frac{1}{\kappa_\pm}$ with $\kappa_\pm < 0$ so that $\mathcal{R}_\pm$ is positive. Now from geometry, we find the relationship

$$R = \frac{\mathcal{R}_+(1-\cos\theta_+)+h_+}{\sin\theta_+},$$

where h_+, θ_+ are as shown in Figure 4. We obtain

$$\frac{\partial R}{\partial \theta_+} = \frac{\mathcal{R}_+ - (\mathcal{R}_+ + h_+)\cos\theta_+}{\sin^2\theta_+}$$

so that upon eliminating h_+ we obtain

$$\frac{\partial R}{\partial \theta_+} = 0 \iff \frac{R}{\mathcal{R}_+} = \tan\theta_+ \tag{69}$$

and similarly with $+$ replaced by $-$. Since $\theta_\pm$ are functions of q_+, we find that at the point where $\frac{dR}{dq_+} = 0$, we have

$$\arctan\frac{R}{\mathcal{R}_\pm} = \theta_\pm.$$

Now from geometry, $\theta_+ = \ell_+/R$, $\theta_- = \ell_-/R$, and $\ell = \ell_+ + \ell_-$. Therefore, upon adding the two equations in (69) we obtain

$$\arctan\frac{R}{\mathcal{R}_+} + \arctan\frac{R}{\mathcal{R}_-} = \theta_+ + \theta_- = \frac{\ell}{R}.$$

But this is precisely (7) with $\lambda_0 = 0$ after substituting $\mathcal{R}_\pm = -\frac{1}{\kappa_\pm}$.

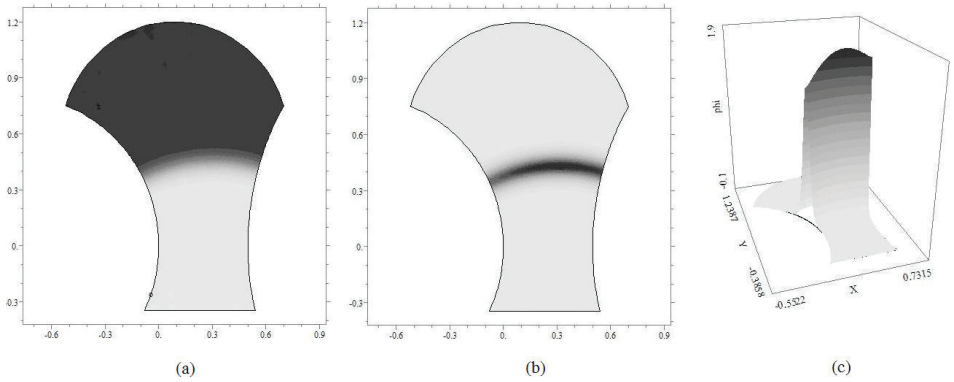

FIG. 5. *Numerical computation of interface and eigenvalue. Left: the steady-state solution $u(x)$ of* (70). *Dark denotes $u \sim 1$ and light denotes $u \sim -1$. Middle: The shape of the corresponding eigenfunction ϕ. Right: surface plot of ϕ. Note the sinusoidal shape along the direction of the interface boundary. Note also a corner layer that is evident near the boundary of the domain. See section* 5 *for parameter values.*

Next, we note that in the case of a cone ($\kappa_+ = \kappa_- = 0$), (7) yields $\lambda_0 = \frac{1}{R^2} > 0$ so that the interface is unstable for a cone domain, for which $R' > 0$. Since λ_0 can only be real, it follows by continuity that λ_0 crosses zero if and only if $R' = 0$, and λ_0 is negative if and only if $R' < 0$. This concludes the proof. ∎

5. Numerical example. We now provide a numerical example of Theorem 2. All computations were done using using the software FlexPDE [19].

Consider a domain as shown in Figure 5. Its left and right boundaries consist of arcs of circles of radii $\mathcal{R}_- = 0.8$, $\mathcal{R}_+ = 1.5$, so that $\kappa_- = -1.25$, $\kappa_+ = -0.667$. The distance between these two boundaries was chosen to be 0.5. The shape of the top and bottom boundaries does not affect the computation as long as they are located $O(1)$ distance from the interface. We chose the nonlinearity to be

$$u_t = \varepsilon^2 \Delta u - 2(u - \varepsilon a)(u-1)(u+1) \tag{70}$$

with $a = 0.55$, $\varepsilon = 0.06$. From Proposition 1 we obtain the theoretical value of the interface radius to be $\hat{R} = \frac{1}{2a} = 0.9091$. To estimate the numerical value of $\hat{R}$, we have used FlexPDE to compute the steady state solution to (70), using $u = \tanh(y/\varepsilon)$ as initial conditions. The resulting steady state is shown on Figure 5(a). Next, we computed the coordinates of the intersection of the middle of the interface ($u = 0$) with the boundary, and then used geometry to obtain $\hat{R}_{\text{numerical}} = 0.9066$. This is in excellent agreement with the theoretical prediction. Geometry then yields an estimate of $l = 0.6486$.

Next, we have solved the eigenvalue problem (4) numerically. Using a global error tolerance of 0.5×10^{-4}, we obtained a numerical estimate of $\lambda_{\text{numerical}} = 0.00504$. This required about 10,000 gridpoints (FlexPDE uses adaptive gridding, and chooses the mesh size based on the global tolerance setting. We have also verified that this result is correct to two significant digits by changing the tolerance). On the other hand, solving (6) gives the theoretical estimate of $\lambda = 0.00506$. Excellent agreement (within 0.5%) is observed.

6. Discussion. In this paper we have characterized the stability of curved interfaces of the perturbed AC system on a bounded domain. On one hand, it is a

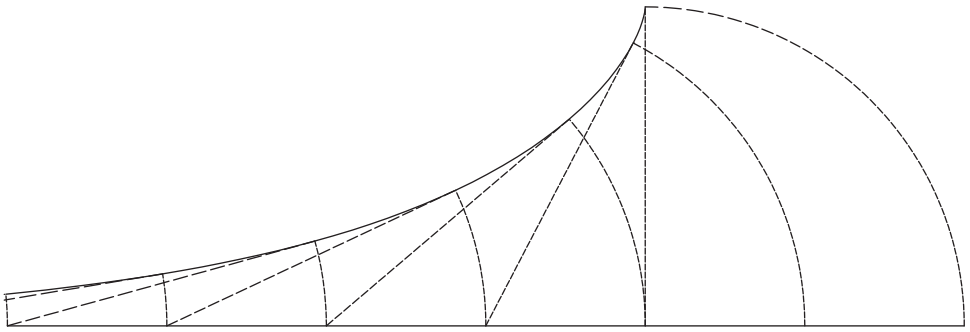

FIG. 6. *A tractrix: the threshold case where all circles intersecting the boundary have identical radius. Theorem* 3 *does not apply to such a domain.*

generalization of the geometric eigenvalue problem derived in [10], [11] for the Allen–Cahn equation without perturbations, which only admits straight interfaces. On the other hand, the perturbed system (1) has been studied on the whole space $\mathbb{R}^2$ without the boundaries—see, for example, [16], [15]. We show that the presence of *both* boundaries and a perturbation can stabilize a curved front. By contrast, the curved front is always unstable in the absence of boundaries—it either shrinks to a point or expands indefinitely depending on the initial conditions [15]. To our knowledge, the characterization of stability that combines both the curvature of the interface and the boundary effect is new.

Algebraically, the stability condition is given by Theorem 2. Geometrically, Theorem 3 states that if $R(s)$ denotes the radius of an arc that intersects the boundary orthogonally at $q_{\pm}(s)$, then the interface is stable if $R'(s) < 0$ whenever $R = \hat{R}$, whereas the interface is unstable if $R'(s) > 0$ at that point (see Figure 2). In particular, this shows explicitly the well-known result that an interface at equilibrium cannot be stable in a convex domain [3]; on the other hand we have shown numerical and theoretical examples where such interface is stable when the domain is nonconvex.

In general, the relationship between the radius R of a circle that intersects the boundary orthogonally and the domain boundary $q = (x, y)$ is given by

$$x = p_1 + R\cos\theta, \quad y = p_2 + R\sin\theta,$$

where $p = (p_1, p_2)$ is the center of the arc of radius R; p_1, p_2, R are arbitrary functions of s; and θ satisfies a differential equation

$$R\frac{d\theta}{ds} = p_1'\sin\theta - p_2'\cos\theta.$$

An interesting threshold case corresponds to $R = \hat{R}$ for all s. If the bottom boundary is the x-axis and $R = \hat{R}$ for all s, then the top boundary forms a *tractrix* (see Figure 6.) This is a well-known curve that is also generated when a ball is dragged on a fixed string by a tractor moving along the x-axis. Implicitly, this curve is given by

$$x = \hat{R}(-t + \tanh(t)), \quad y = \hat{R}\,\mathrm{sech}(t).$$

It is an open problem to describe either the stability or the location of the interface for such a domain.

An interesting conjecture arises in studying the propagation of fronts around a concave corner. Such domains were used in [17], where the propagation of chemical

fronts was considered. An interface passing through the corner may get "stuck" at the corner or go through it, depending on the geometry. If we "smooth out" the corner and take ε sufficiently small, then we can apply Theorem 3. The result is that the interface will get stuck at the corner if there exists a circle that intersects orthogonally with one boundary, and that passes through the corner point, and whose radius is at most $\hat{R}$. This is essentially the geometrical condition described in section III.B in [17] and it agrees well with numerical results presented there. However, the construction of an interface at a corner point is an open theoretical problem.

REFERENCES

[1] N. Alikakos, G. Fusco, and M. Kowalczyk, *Finite dimensional dynamics and interfaces intersecting the boundary: Equilibria and the quasi-invariant manifold*, Indiana Univ. Math. J., 45 (1996), pp. 1119–1156.

[2] S. Allen and J. W. Cahn, *A microscopic theory for antiphase boundary motion and its application to antiphase domain coarsening*, Acta. Metall., 27 (1979), pp. 1084–1095.

[3] R. G. Casten and J. Holland, *Instability results for reaction diffusion equations with Neumann boundary conditions*, J. Differential Equations, 27 (1978), pp. 266–273.

[4] G. Chapuisat and E. Grenier, *Existence and nonexistence of traveling wave solutions for a bistable reaction-diffusion equation in an infinite cylinder whose diameter is suddenly increased*, Comm. Partial Differential Equations, 30 (2005), pp. 1805–1816.

[5] X. Chen, *Generation and propagation of inerfaces in reaction-diffusion equations*, J. Differential Equations, 96 (1992), pp. 116–141.

[6] M. del Pino, M. Kowalczyk, and J. Wei, *Resonance and interior layers in an inhomogeneous phase transition model,* SIAM J. Math. Anal., 38 (2007), pp. 1542–1564.

[7] P. C. Fife and J. B. MacLeod, *The approach of solutions of nonlinear diffusion equations to travelling front solutions*, Arch Ration. Mech. Anal., 65 (1977), pp. 335–361.

[8] P. Fife and W. M. Greenlee, *Interior transition layers for elliptic boundary value problems with a small parameter,* Russian Math. Surveys, 29 (1974), pp. 103–131.

[9] T. Ilmanen, *Convergence of the Allen-Cahn equation to the Brakkke's motion by mean curvature*, J. Differential Geom., 38 (1993), pp. 417–461.

[10] M. Kowalczyk, *Approximate invariant manifold of the Allen-Cahn flow in two dimensions*, in Partial Differential Equations and Inverse Problems, Comptemp. Math. 362, Amer. Math. Soc., Providence, RI, 2004, pp. 233–239.

[11] M. Kowalczyk, *On the existence and Morse index of solutions to the Allen-Cahn equation in two dimensions*, Ann. Mat. Pura Appl., 184 (2005), pp. 0373–3114.

[12] R. Kohn and P. Sternberg, *Local minimizers and singular perturbations*, Proc. R. Soc. Edinburgh, 111 A (1989), pp. 69–84.

[13] H. Matano, *Asymptotic behavior and stability of solutions of semilinear diffusion equations*, Publ. Res. Inst. Math. Sci., 15 (1979), pp. 401–454.

[14] F. Pacard and M. Ritore, *From constant mean curvature hypersurfaces to the gradient theory of phase transition*, J. Differential Geom., 64 (2003), pp. 359–423.

[15] L. Pismen, *Patterns and Interfaces in Dissipative Dynamics,* Springer Verlag, 2006, p. 374.

[16] J. Rubinstein, P. Sternberg, and J. B. Keller, *Fast reaction, slow diffusion, and curve shortening*, SIAM J. Appl. Math., 49 (1989), pp. 116–133.

[17] L. Qiao, I. G. Kevrekidis, C. Punckt, and H. H. Rotermund, *Guiding chemical pulses through geometry: Y junctions*, Phys. Rev. E, 73 (2006), 036219.

[18] M. Ward and D. Stafford, *Metastable dynamics and spatially inhomogeneous equilibria in dumbbell-shaped domains*, Studies in Appl. Math., 103 (1999), pp. 51–73.

[19] See FlexPDE website, www.pdesolutions.com.